Wintertime CO_2 Fluxes in an Arctic Polynya Using Eddy Covariance: Evidence for Enhanced Air–Sea Gas Transfer During Ice Formation

B.G.T. Else,[1] T.N. Papakyriakou,[1] R.J. Galley,[1] W.M. Drennan,[2] L.A. Miller,[3] H. Thomas[4]

[1]Centre for Earth Observation Science, Department of Environment and Geography, University of Manitoba, Winnipeg, Manitoba, Canada.

[2]Division of Applied Marine Physics, Rosenstiel School of Marine and Atmospheric Science, University of Miami, Miami, Florida, USA

[3]Centre for Ocean Climate Chemistry, Institute of Ocean Sciences, Fisheries and Oceans Canada, Sidney, British Columbia, Canada

[4]Department of Oceanography, Dalhousie University, Halifax, Nova Scotia, Canada

Abstract.

Between Nov. 1 2007 and Jan. 31 2008, we calculated the air–sea flux of CO_2, sensible heat, and water vapour in an Arctic polynya system (Amundsen Gulf, Canada) using eddy covariance equipment deployed on the research icebreaker *CCGSAmundsen*. During this time period, Amundsen Gulf was a dynamic sea ice environment composed primarily of first year ice with open water coverage varying between 1–14%. In all cases where measurements were influenced by open water we measured CO_2 fluxes that were 1–2 orders of magnitude higher than those expected under similar conditions in the open ocean. Fluxes were typically directed towards the water surface with a mean flux of -4.88 μmol m^{-2} s^{-1} and a maximum of -27.95 μmol m^{-2} s^{-1}. One case of rapid outgassing (mean value +2.10 μmol m^{-2} s^{-1}) was also observed. The consistent patten of enhanced gas exchange over open water allows us to hypothesize that high water–side turbulence is the main cause of these events. Modification of the physical and chemical properties of the surface seawater by cooling and brine rejection may also play a role. A rough calculation using an estimate of open water coverage suggests that the contribution of these events to the annual regional air–sea CO_2 exchange budget may make the winter months as important as the open water months. Although high, the uptake of CO_2 fits within mixed layer dissolved inorganic carbon budgets derived for the region by other investigators.

1. Introduction

In order to properly forecast the effects of climate change, general circulation models need to adequately account for sources and sinks of CO_2. The global marine system plays a major role in cycling CO_2 and presently absorbs about 2.2 PgC year^{-1}[*Denman et al.*, 2007], which offsets about 30% of present anthropogenic emissions. However, the rate of CO_2 uptake is not consistent across all oceans. On an annual basis a given region may behave anywhere on the spectrum from a strong source of CO_2 to a strong sink, and significant inter- and intra-annual variability may also exist [*Takahashi et al.*, 2009]. This spatio-temporal variability arises from variability in the processes controlling CO_2 fluxes.

For the open ocean, research has advanced to the point where these processes are known well enough to make reasonable flux estimates at a wide range of scales (see review by *Wanninkhof et al.* [2009]). Typically, estimates of CO_2 flux (F_{CO_2}) are computed using a form of the bulk flux equation:

$$F_{CO_2} = \alpha k(p\mathrm{CO}_{2sw} - p\mathrm{CO}_{2air}) \tag{1}$$

where α is the solubility of CO_2 in water, $p\mathrm{CO}_{2sw}$ is the partial pressure of CO_2 in the surface seawater, $p\mathrm{CO}_{2air}$ is the partial pressure of CO_2 in the atmosphere and k is the gas transfer velocity. Using this approach, the air-sea gradient of CO_2 ($p\mathrm{CO}_{2sw} - p\mathrm{CO}_{2air}$, commonly denoted $\Delta p\mathrm{CO}_2$) determines the potential for exchange, while the transfer velocity encompasses the processes that control the rate at which the exchange can occur. The main determinant of transfer velocity is water-side turbulence, which itself is mainly determined by wind velocity through its relationship with momentum flux [*Jähne*, 1987].

Many other factors influence water-side turbulence, such as wave state [*Bock et al.*, 1999; *Zappa et al.*, 2004], surface films [*Jähne*, 1987; *Frew et al.*, 2004; *Frew*, 1997], rain [*Ho et al.*, 2004; *Takagaki and Komori*, 2007; *Zappa et al.*, 2009], tides [*Zappa et al.*, 2007], and buoyancy [*McGillis et al.*, 2004]. In addition, several processes not directly related to turbulence also affect transfer velocity, such as chemical enhancement [*Bolin*, 1960; *Kuss and Schneider*, 2004] and bubbles from breaking waves [*Asher et al.*, 1996; *Woolf*, 1997; *Woolf et al.*, 2007]. Despite the myriad processes affecting gas exchange, wind velocity alone is typically used to estimate transfer velocity in the open ocean with mature wave fields [*Wanninkhof et al.*, 2009]. As such, numerous parameterizations to estimate k from wind speed have been created based on tank experiments [*Liss and Merlivat*, 1986], modelling exercises [*Wanninkhof*, 1992; *Sweeney et al.*, 2007], and field studies conducted primarily at low and mid–latitudes [*Ho et al.*, 2006; *Nightingale et al.*, 2000; *Wanninkhof and McGillis*, 1999].

At high latitudes (e.g. the Arctic), the processes that control CO_2 fluxes are not well known. Depending on the season and location, a given region of the Arctic Ocean may be ice free or it may be covered by sea ice of variable concentration, thickness and thermodynamic state. During the open water season it is reasonable to assume that what we understand about open-ocean fluxes would be applicable, but as soon as sea ice is present existing parameterizations of transfer velocity are likely invalid. Although sea ice is permeable to gas exchange under certain conditions [*Gosink et al.*, 1976], the mechanisms that control the rate of exchange are very different from the open ocean. Furthermore, the open water that does remain in an icescape experiences different controls on near-surface turbulence; fetch limitations [*Woolf*, 2005] imposed by surrounding ice floes and the generation of turbulence due to ice formation [*McPhee and Stanton*, 1996] are two examples of those unique controls.

The initial freeze-up and growth of sea ice has generated considerable interest, since the process significantly modifies the chemistry of the surface ocean and because dissolved inorganic carbon (DIC) may be driven down from the surface with rejected brines in what has been termed a sea ice CO_2 pump [*Rysgaard et al.*, 2007, 2009; *Anderson et al.*, 2004] . A water column study by *Anderson et al.* [2004] in Svalbard found high DIC and elevated chlorofluorocarbon levels in deep waters, which they hypothesized originated from enhanced air-sea exchange of CO_2 during ice formation. Some support for this enhanced exchange was recently presented in a tank study by *Loose et al.* [2009]. In this paper, we describe the first eddy covariance observations of such flux enhancements over a natural sea ice surface.

2. Study Area

The data presented in this paper were collected between Nov. 1, 2007 and Jan. 31, 2008 during the International Polar Year Circumpolar Flaw Lead System Study (CFL) in Amundsen Gulf and the southeaster Beaufort Sea (Figure 1). The region is subject to a complex annual ice cycle which has been summarized by *Galley et al.* [2008]. The open water season (defined as sea ice concentration $\leq 20\%$) typically lasts 10 weeks, starting in late July. Freeze-up occurs in early October and is characterized by initial landfast ice growth along the coastal margins. The ice which forms offshore in Amundsen Gulf typically remains mobile during the time period of this study (shaded areas in Figure 1), creating an icescape which is characterized by small transient leads and polynyas. Later in the winter the eastern half of Amundsen Gulf may become landfast, and on some occasions the western portion becomes landfast as well. The Beaufort Sea pack ice remains mobile throughout the winter, rotating with the predominant Beaufort gyre to create persistent linear flaw lead features (Figure 1). The mean spring breakup for Amundsen Gulf is early June, which creates the feature commonly referred to as the Cape Bathurst polynya (Figure 1) which in some years extends well into eastern Amundsen Gulf.

Observations have shown that the region experiences significant air-sea $p\mathrm{CO}_2$ gradients in the fall. *Mucci et al.* [2010] observed $\Delta p\mathrm{CO}_2$ ranging from -138 to -28 μatm from Sep.–Nov. 2003, and *Murata and Takizawa* [2003] observed gradients of similar magnitude during three years of cruises in Aug.–Sep., 1998–2000. Observations made during the CFL study showed that significant undersaturation ($\Delta p\mathrm{CO}_2$ typically around -70 μatm) persisted through the end of January 2008 in offshore Amundsen Gulf [*Shadwick et al.*, 2011].

During the winter season, the persistent flaw leads and polynyas in combination with strong local $p\mathrm{CO}_2$ gradients make this study area an ideal location for examining the effect of freezing sea ice on gas exchange.

3. Methods

3.1. Atmospheric Instrumentation

For the duration of the experiment a guyed open-lattice tower at the bow of the ship was instrumented with eddy covariance and meteorological equipment. The flux instrumentation consisted of a Gill Windmaster Pro sonic anemometer/thermometer, a LI-COR LI-7500 open path CO_2/H_2O gas analyzer and a Systron Donner MotionPak. The flux instrumentation was located at a height of 14 m above the surface (7 m above the deck of the ship), with the exception of the MotionPak which was located at the midpoint of the tower.

The meteorological equipment consisted of a conventional anemometer for wind speed and direction (RM Young 05103, height=15 m), a temperature/relative humidity probe (Vasailla HMP45C212, height=14 m) and a pressure sensor (RM Young 61205V). An array of radiation sensors was deployed on top of the wheelhouse of the ship, consisting of a photosynthetically active radiation (PAR) sensor (Kipp & Zonen PARlite), an incoming shortwave radiation sensor (Eppley PSP) and an incoming longwave radiation sensor (Eppley PIR).

3.2. Surface Water pCO$_2$ Instrumentation

Surface water from a dedicated scientific intake line (depth ∼5 m) was continuously sampled for pCO_{2sw} using a shower-type equilibrator which cycled headspace air through a LI-COR LI-7000 CO_2/H_2O gas analyzer [*Körtzinger et al.*, 1996]. The gas analyzer was calibrated daily using ultra-high purity N_2 as a zero gas and a CO_2/air mixture traceable to WMO standards as a span gas. The instrument was located in the engine room very close to the water intake, but a slight warming of the sample water relative to results from CTD casts was detected by a thermocouple in the equilibrator. This warming effect was very consistent, allowing correction of pCO_{2sw} for thermodynamic effects following *Takahashi et al.* [1993]. After correction, the pCO_{2sw} measurements showed good agreement ($r^2 = 0.9$, mean difference = 19 μatm, no statistically significant bias) with independent calculations from DIC/TA measurements (see *Shadwick et al.* [2011] for a description of the DIC/TA dataset and methods).

3.3. Study Design

The CFL study was a unique over-wintering experiment because the research vessel remained mobile through the entire winter. The goal of this strategy was to create a time series of the seasonal evolution of the flaw lead/polynya system. Logistically, this meant that the specific location and operation of the vessel was highly opportunistic; when ice conditions allowed ship to move freely, spatial sampling was conducted, but when ice conditions were more severe the ship was positioned in large consolidated floes and allowed to drift. These floes were typically occupied for 1 – 7 days, depending on the stability of the floe and whether or not it was drifting outside of the study area. When repositioning was necessary, the ship would break out of the floe and either break ice or transit through small flaw leads until a more suitable floe was located.

3.4. Eddy Covariance

The study design allowed us to examine a sea ice system which would otherwise be inaccessible, but it does have implications for the eddy covariance technique which is best suited for a stationary tower over a homogenous surface. To help address these issues, we filtered the data to ensure that each eddy covariance run was not subject to significant changes either in ship operation or atmospheric conditions. If the ship was under power, ship velocity and course over ground were required to be consistent (within $\pm$ 3.7 km hr^{-1} of mean for velocity and $\pm$ 27.5° of mean for course). Relative wind direction was also required to be consistent within $\pm$27.5° of the mean, and it was further restricted to within $\pm$ 90° of the bow of the ship to reduce the effects of flow distortion. To help with the issue of non–homogeneous surfaces, we found it useful to break the data up into individual case studies during time periods where flux data collection was consistent and the ship location, atmospheric conditions and sea ice conditions were fairly uniform (see Table 1, Figure 2).

Filtering was also necessary to remove instances where atmospheric conditions negatively impacted the flux instruments. The LI-7500 outputs a diagnostic value that warns of lens obstruction, which during this study was most often caused by accretion of rime. We filtered out all instances where the diagnostic value exceeded its normal operating range, creating a fairly significant loss of data. The sonic anemometer was less influenced by riming, but filtering was carried out based on the characteristically erratic performance of the instrument that occurs under such circumstances.

The LI-7500 used in this study makes high frequency (10Hz) measurements of the molar concentrations of CO_2 and water vapour (c_{co_2} and c_v respectively). By combining these measurements with high frequency vertical wind velocity (w) measurements from the sonic anemometer, the flux of CO_2 is calculated over an averaging period (in this case, 30 minutes) via:

$$F_c = \overline{w'c'_{co_2}} + \frac{\overline{c}_{co_2}}{\overline{c}_d}\left[\overline{w'c'_v} + \overline{c_a}\frac{\overline{w'T'}}{\overline{T}}\right] \tag{2}$$

where the overbars denote averaged quantities, the primes indicate fluctuations around a mean value, T is air temperature, c_d is the dry air molar concentration, and c_a is the moist air molar concentration [*Leuning*, 2004]. The second term on the right hand side of equation 2 is the so-called WPL correction (or dilution correction) that must be used for open path sensors [*Webb et al.*, 1980]. The necessary high frequency T measurements are determined from sonic temperature (measured by the sonic anemometer), which were converted to T following *Kaimal and Gaynor* [1991]. The MotionPak provides 3-axis measurements of acceleration and angular velocity which were used to correct w for ship motion. The techniques for this correction were first adapted for ships by *Mitsuta and Fujitani* [1974], and later refined by other investigators [*Fujitani*, 1981; *Dugan et al.*, 1991; *Anctil et al.*, 1994; *Edson et al.*, 1998].

The utility of open path sensors for measuring CO_2 fluxes has recently been debated for conditions where low fluxes are expected [*Burba et al.*, 2008; *Amiro*, 2010; *Ono et al.*, 2008] and in the marine environment [*Prytherch et al.*, 2010]. During the non-growing season over several terrestrial ecosystems, significant uptakes of CO_2 have been observed and identified as artifacts of the LI-7500 gas analyzer [*Amiro*, 2010; *Ono et al.*, 2008; *Hirata et al.*, 2007]. Work by *Burba et al.* [2008] have shown that a heat flux generated by the electronics of the LI-7500 is likely the most significant contributor to this bias, especially at low air temperatures. Other suggestions include pressure fluctuations at high wind velocities that are not usually included in the WPL correction [*Järvi et al.*, 2009] and incomplete WPL corrections due to poor energy balance closure [*Ono et al.*, 2008]. The magnitude of these discrepancies are usually on the order of 1 μmol m^{-2} s^{-1}, which in most terrestrial systems during the growing season is a small percentage of the total flux. However, typical magnitudes of CO_2 flux in the open ocean are less than 1 μmol m^{-2} s^{-1} (e.g., *McGillis et al.* [2001]).

A further difficulty of working with an open path analyzer in a marine environment is an apparent sensitivity to contamination of the sensor lens by impurities (most likely salt particles) [*Kohsiek*, 2000; *Prytherch et al.*, 2010]. The contamination appears to cause a portion of water vapour fluctuations to be mis–recorded as fluctuations of CO_2 (an effect known as "crosstalk"), and can lead to CO_2 fluxes an order of magnitude higher than expected [*Prytherch et al.*, 2010].

Corrections have been proposed for both the sensor heating and H_2O crosstalk issues. *Burba et al.* [2008] proposed several ways in which the heat flux of the LI-7500 can be estimated and added to the WPL correction. In this study, we have adopted their multivariate regression model for determining the sensor heat flux from air temperature, wind velocity and incoming longwave/shortwave radiation. *Prytherch et al.* [2010] proposed a correction for the H_2O crosstalk (termed the "PKT" correction) in which an iterative approach is used to remove unwanted correlation between the CO_2 and H_2O signals. This correction has also been adopted for this study, but as we discuss in section 5.1 we found it to be unreliable. Thus, all CO_2 flux values reported herein include only the *Burba et al.* [2008] correction along with the usual WPL corrections.

3.5. RADARSAT-1 Imagery

To aid in the identification of ice conditions and to quantify the amount of open water within the study area over the period, fourteen (14) RADARSAT-1 ScanSAR narrow beam images acquired between Nov. 6 2007 and Jan. 28 2008 were classified. RADARSAT-1 ScanSAR narrow beam mode has a resolution of 50 m and a nominal coverage area of 300 x 300 km. Each of the images were geo-referenced and calibrated to $\sigma°$, then geographically cropped using latitudinal bounds 70° and 71.5°N and longitudinal bounds 122° and 126°W. The calibrated, geo-referenced sub-images were then subjected to a median filter with a 3x3 window size to reduce the "speckle" noise common to synthetic aperture RADAR (SAR) imagery while preserving edges. Edge preservation is very important when linear features such as leads are the predominant form of open water at this time of year. Finally, each sub-image was manually classified according to the principles set forth by the Canadian Ice Service (CIS) SAR ice interpretation guide [*Canadian Ice Service*, unpublished].

4. Results

4.1. Observations of High CO_2 Flux Events

4.1.1. Case 1: Nov. 2 04:30 - Nov. 3 09:30

On Nov. 2, the ship conducted a transect across the mouth of Amundsen Gulf. A RADARSAT-1 image was acquired on Nov. 2 at 01:54 (all times herein reported as UTC) just prior to the start of the transect, which clearly shows that the region was a mix of open water, old ice floes, and newly forming grease ice (Figure 3). Due to the ice in the area the intake line for the $p\mathrm{CO}_{2sw}$ system was clogged so that we could not obtain measurements of $\Delta p\mathrm{CO}_2$. However, samples collected in the region in the previous two days showed that the $\Delta p\mathrm{CO}_2$ was around -80 μatm.

Over this time period, we measured a flux of up to -4.26 μmol m^{-2} s^{-1}, with a mean value of -1.81 μmol m^{-2} s^{-1}. Associated with this strong CO_2 uptake was a high sensible heat flux from the ocean to the atmosphere (up to 100 W m^{-2}, mean of 43.3 W m^{-2}, Figure 4b). This heat flux must have been driven by open water, over which a strong temperature gradient forms due to the relative warmth of the ocean. We therefore interpret the strong CO_2 fluxes to likewise be a signal of open water gas exchange.

4.1.2. Case 3: Nov. 20 01:30 – 14:45

The second instance where we observed particularly high CO_2 fluxes was on Nov. 20, near the southern tip of Banks Island. At this point ice concentration in Amundsen Gulf was very high, and the ship was parked in a 36 cm thick ice floe. Prior to this time, a strong wind event from Nov. 16-17 (wind velocities peaking at about 24 m s^{-1}) created significant ice motion and fracture in the region. This was followed by very low winds (about 5 m s^{-1}), allowing the open water features to appear obviously on a RADARSAT-1 image acquired on Nov. 20 at 01:29 as dark features (Figure 5). Early on Nov. 20, easterly winds picked up quickly to about 13 m s^{-1} and persisted through the sample case (Figure 6c). This wind induced significant ice motion (the ship drifted at a mean velocity of 0.6 km hr^{-1}, increasing steadily from 0.4 to 1.1 km hr^{-1}), which would have expanded the open water leads. A signal of open-water fluxes was clearly evident in the heat flux measurements, reaching nearly +100 W m^{-2} (Figure 6b) with a mean value of +53.8 W m^{-2} (Table 1).

During this case, rapid outgassing of CO_2 was observed at a mean rate of +2.10 μmol m^{-2} s^{-1}. The outgassing was somewhat surprising given that the $p\mathrm{CO}_{2sw}$ system recorded undersaturation of -75 μatm (Table 1), but the surface water upwind of the ship may have been supersaturated. This result shows that at times our eddy covariance measurements (which are an integrated flux from the upwind surfaces) are difficult to reconcile with the $p\mathrm{CO}_{2sw}$ data (which measures at the same location as the tower).

4.1.3. Case 4: Nov. 20 16:00 – 18:30

Case 4 is an extension of Case 3, but we split the two because the ship repositioned (approximately 1.5 km north) to a new ice floe (Figure 5), and the CO_2 flux changed markedly. The heat flux measurements from Case 4 were still heavily influenced by an open water signal, with even higher values than in case 3 (mean and maximum values of +111.4 and +140.7 W m^{-2} respectively, Figure 6b). This is in agreement with ship-board observations that the area was a mixture of ice and open water under strong wind forcings.

After the ship repositioned, a very strong negative flux of CO_2 was observed (mean and maximum values of -9.58 and -11.43 μmol m^{-2} s^{-1} respectively, Figure 6a). This flux direction is in better agreement with the $\Delta p CO_2$ gradient observed in the area, and may be a result of a change in the upwind surface to lower (i.e. undersaturated) pCO_{2sw} as the ship moved around the southern tip of Banks Island (Figure 5).

4.1.4. Case 7: Dec 1 07:00 – 12:30

The strongest CO_2 fluxes that we measured were on Dec. 1 during a transit along the southwest coast of Banks Island. Immediately prior to this transit, the ship was drifting south in an ice floe under fairly high winds (mean 11.8 m s^{-1}). This drifting event made up Case 6, where no strong CO_2 fluxes or heat fluxes were observed (Table 1). The ship eventually broke out of this drift, and transited through an active wind-roughened flaw lead. This flaw lead event was captured in a RADARSAT–1 image taken shortly after the end of case 7 (Dec. 1, 14:45, Figure 7).

The transit was very short, and only four 30 minute samples passed our quality control tests. However, all of these samples showed very high CO_2 uptake, with flux values ranging from -9.33 to -27.95 μmol m^{-2} s^{-1} (Figure 8a). Once again, these fluxes were accompanied by high sensible heat fluxes indicative of open water (Figure 8b). No pCO_{2sw} measurements were available during the transit due to a clogged intake line, but based on the $\Delta p CO_2$ during the cases bracketing this one (-52.1 and -63.6 μatm for cases 6 and 8, respectively, Table 1), the direction of the flux appeared to be in agreement with the gradient.

4.1.5. Case 17: Jan 24. 08:00 - Jan. 25 05:30

The final instance where we measured unusually strong CO_2 fluxes was during case 17 in late January. During this time, the ship was drifting in an ice floe with a thickness of about 100 cm. A RADARSAT image collected at 01:33 on Jan. 24 showed considerable fracturing upwind of the ship (Figure 9).

This case was characterized by high wind velocities (up to 19 m s^{-1}, Figure 10c) which caused ice drift up to 1.4 km hr^{-1}. These strong winds and ice motion drove significant open water, as observed in heat flux measurements approaching 100 W m^{-2} (Figure 10b). Associated with this sensible heat signal was a strong, consistent CO_2 uptake (Figure 10a) with a mean flux of -3.15 μmol m^{-2} s^{-1}, in agreement in direction with an observed $\Delta p CO_2$ gradient of -38.5 μatm.

4.2. Observations of Low CO_2 Fluxes

4.2.1. Observations in Land Fast Ice

Flux measurements were made in land fast sea ice on three occasions: case 2 (Nov. 8 02:15 – Nov. 9 00:50, 69.50 °N/123.93 °W), case 8 (Dec. 1 13:45 – Dec. 2 02:45, 71.90 °N/125.44 °W), and case 11 (Dec. 19 23:15 – 18:15, 71.91 °N/125.43 °W). The minimum ice thickness for all of these samples was an estimated 40 cm (case 2), and the ice was much thicker (approaching 100 cm) in the other two cases. Sensible heat flux in all cases was small (Table 1), and in all three cases the wind direction was such that the upwind fetch was composed of fast ice. This suggests that what we were measuring was indeed a land fast ice signal. In these cases, mean fluxes were between +0.23 – +0.42 μmol m^{-2} s^{-1} (Table 1 and Figure 2). If these measurements are reliable, they would suggest a flux of CO_2 at a climatologically significant rate. However, we will show in section 5.1 that these low fluxes likely cannot be distinguished from the noise and biases inherent in our eddy covariance system.

4.2.2. Observations in High Concentration Mobile Ice

A second scenario in which we typically observed non-resolvable CO_2 fluxes was when the ship was drifting in highly concentrated mobile sea ice. These conditions were observed during case 6 (Nov. 30 05:15 – 23:00), case 9 (Dec. 2 05:30 – 22:15), case 13 (Jan. 2 18:15 – Jan. 6 03:30), case 14 (Jan. 10 09:15 – Jan. 11 18:45), case 15 (Jan. 13 16:00 – Jan. 14 00:00) and case 16 (Jan. 20 17:00 – Jan. 21 04:30). As Table 1 shows, all of these cases had very low sensible heat fluxes (highest mean flux was +3.2 W m^{-2}, case 15), and mean CO_2 fluxes ranged from -0.50 – +0.58 μmol m^{-2} s^{-1} (Table 1, Figure 2).

4.2.3. Observations in Thin Ice

A final scenario which is perhaps more interesting is the observation of non-detectable CO_2 fluxes in cases where other observations (field data and heat flux measurements) suggest that thin ice may be present. Only case 10 (Dec. 4 23:00 – Dec. 6 12:15) falls into this category. RADARSAT–1 images (not shown) acquired shortly before (Dec. 4, 01:21) and after this run (Dec. 7 01:33) do not show a lot of obvious thin ice, but ice cores taken from the surrounding floe were only 26 cm thick. The heat flux measurements (Figure 11b) were consistently positive (mean value of +15.8 W m^{-2}), but lower than those observed in section 4.1. Thin ice transfers heat at significant rates, but does so less vigorously than open water [*Maykut*, 1978]. Although winds were moderate (5 – 7 m s^{-2}, Figure 11c) the $\Delta p CO_2$ gradient was quite high (mean value of -86.7 μatm). If a flux enhancement was occurring similar to those described in section 4.1, we would expect to be able to detect it in our CO_2 flux measurements. However, Figure 11a clearly shows that fluxes were not distinctly above the uncertainty inherent in the system. These findings suggest that open water – not just thin ice – is required to drive CO_2 flux at the levels shown in section 4.1.

5. Discussion

5.1. Sensor Uncertainties

The results obtained in land fast and consolidated ice (sections 4.2.1 & 4.2.2) provide an opportunity to test the noise and bias inherent in our eddy covariance system. There is in fact good reason to expect that CO_2 fluxes over these surfaces (thick, cold, consolidated sea ice) should be zero. At surface ice temperatures below ~-5°C and typical brine salinity, the brine volume drops below 5% which inhibits liquid transport through the ice [*Golden et al.*, 1998]. *Loose et al.,* [2010] examined the transport of gases near this liquid transport threshold, and found the gas transfer velocity to be very small relative to seawater. Similarly, *Nomura et al.,* [2006] measured small CO_2 fluxes (maximum ∼ $+0.01\mu$mol m^{-2} s^{-1}) over thin laboratory ice well above the liquid transport threshold. At ice temperatures that reduce brine volume to below 5%, these small rates of gas exchange should be effectively shut off.

After Nov. 28, 2007 (when most of the measurements described in sections 4.2.1 & 4.2.2 were made) surface ice temperatures were consistently well below -5°C and brine volumes were typically below 5% [G. Carnat, unpublished data]. We would therefore expect any deviation of the mean CO_2 fluxes over these surfaces from zero to be indicative of bias, and any variation around that mean to be noise in the measurement system. To this end, we calculated the mean and standard deviation of the raw, sensor heating corrected, and crosstalk (PKT) corrected CO_2 fluxes from cases 2, 6, 8, 9, 11 & 13–16 (Table 2).

The uncorrected fluxes show a negative bias (-0.45 μmol m^{-2} s^{-1}), which is in the direction predicted by both sensor heating and water vapour crosstalk effects. The standard deviation of CO_2 fluxes around this mean was 0.76 μmol m^{-2} s^{-1}, indicating that noise is quite high in the system. By applying only the sensor heating correction, the bias moved to +0.13 μmol m^{-2} s^{-1} – a reduction in the magnitude of the bias, but a slight overcorrection. Fortunately, this correction did not add a lot of additional noise to the system, as the standard deviation remained relatively unchanged (0.77 μmol m^{-2} s^{-1}).

The PKT correction, however, was more troublesome. We found that 55% of the samples from these cases produced what we determined to be an "unreasonable" correction (magnitude of correction >5.5 μmol m^{-2} s^{-1}). Of the remaining samples, the net effect of the correction was to actually make the CO_2 flux more negative, counter to the expected direction. Furthermore, the correction added additional noise as evidenced by an increase in standard deviation to 1.30 μmol m^{-2} s^{-1}. Since no negative bias remains in the mean flux after the sensor heating correction, we conclude that crosstalk contamination must have been small for our system even prior to applying the PKT correction. Arguments for a low crosstalk error in this environment have a strong physical basis, because latent heat fluxes were very small (typically <5 W m^{-2}) compared to the examples discussed by *Prytherch et al.* [2010] ($\sim$60 W m^{-2}). From an eddy covariance standpoint, a low latent heat flux means that water vapour is not highly correlated with vertical wind velocity, and thus should not cause significant spurious correlation between CO_2 and vertical wind velocity. For these reasons, we decided not to include the PKT correction in our results.

We propose that our system has an overall uncertainty of $\pm$0.77 μmol m^{-2} s^{-1} and a bias of +0.13 μmol m^{-2} s^{-1} based on the results of the sensor heating corrected fluxes.

This level of uncertainty shows that our measurements of high CO_2 flux (section 4.1) are above the noise level of the system, and are not the result of a strong systematic bias.

5.2. Enhanced Gas Flux by Sea Ice Formation

Our results from section 4.1 indicate that in the winter mixed ice environment of the Amundsen Gulf, the presence of open water drives a very rapid exchange of CO_2. For comparison, under the typical $\Delta p CO_2$ (∼-70 μatm) and wind velocity (∼8 ms^{-1}) conditions we encountered, the bulk flux approach (equation 1) would predict fluxes in the range of -0.10 to -0.12 μmol m^{-2} s^{-1}. Even using the maximum wind velocities observed (19 ms^{-1}), we would not expect fluxes to exceed about -1.5 μmol m^{-2} s^{-1}. Our measured fluxes are therefore at times 1–2 orders of magnitude higher than what might be expected under similar conditions in the open ocean.

Several authors have suggested that an enhancement of gas exchange due to sea ice formation may exist [*Anderson et al.*, 2004; *Rysgaard et al.*, 2007; *Loose et al.*, 2009], but none have described in detail the physical and chemical processes which may account for it. Our study likewise lacks the necessary ancillary observations to show conclusively what processes are responsible for enhanced gas transfer, but in this section we propose two key hypotheses to explain it: (1) enhanced water side turbulence driven by rapid cooling and brine rejection, and (2) modification of the carbonate system of the surface seawater. These hypotheses are summarized in Figure 12 and discussed below.

5.2.1. Enhanced Water Side Turbulence

At the upwind side of a flaw lead, a significant heat flux occurs due to the exposure of the relatively warm (i.e. ∼ -1.8 °C) water to the very cold atmosphere (∼ -10 – -25 °C). This cooling creates a destabilization of the water surface and generates buoyancy fluxes that may enhance turbulence. *McGillis et al.* [2004] observed a 40% enhancement of CO_2 fluxes during modest nighttime cooling (sensible heat fluxes on the order of 1-10 W m^{-2}) in the equatorial pacific, which was attributed mostly to these buoyancy fluxes. In a situation such as the one shown in Figure 12 where sensible heat fluxes are 1–2 orders of magnitude higher, this enhancement is likely to be much more pronounced.

A second process that may drive high turbulence is the rejection of dense brines by frazil ice formation. Frazil ice is small, unconsolidated ice crystals that are primarily generated just below the surface [*Ushio and Wakatsuchi*, 1993]. It is easily transported away from the open water site, creating a region of rapid ice formation but persistent open water. Frazil ice crystals are thought to be essentially pure [*Omstedt*, 1985] which means that their formation results in the rejection of any solutes, which must create density instabilities and drive enhanced turbulence similar to the effect of heat loss.

Unfortunately, turbulence in these systems has not been well studied. Between Nov. 16 – Dec. 18, one of our collaborators collected 175 profiles of turbulent kinetic energy dissipation rate (ϵ) from a minimum depth of 10 m using a vertical microstructure turbulence profiler (VMP, see *Bourgault et al.* [2008] for instrument details). ϵ at 10 m reached values of $O(10^{-5})$ W kg^{-1} on a few ($\sim$ 4) profiles, with an approximately exponential decrease with depth [D. Bourgault, pers. comm]. Extrapolating above 10 m suggests surface dissipation rates that may have occasionally reached $O(10^{-4})$ W kg^{-1}. These values are considerably higher than ϵ measured under refrozen leads at a similar depth by *McPhee and Stanton* [1996] ($O(10^{-8})$ – $O(10^{-7})$ W kg^{-1}). The exponential shape of the dissipation measurements points to surface turbulence generation, but given that the dominant ice cover must restrict wind and wave action, sea ice processes (likely including ice drift and brine rejection) must play an important role in this system. *Zappa et al.* [2007] showed that ϵ is a better predictor of gas transfer velocity than wind in systems where turbulence is generated from other sources. Our maximum predicted surface ϵ values are similar to the highest ϵ measurements made by *Zappa et al.* [2007] in coastal zones and tidal estuaries, but they are not high enough to account for the rate of gas transfer we observed. However, the VMP was almost always deployed when the ship was stationary in ice floes, and it therefore may not have captured the nature of the transient flaw leads that we hypothesize to be the cause of our high observed CO_2 fluxes.

5.2.2. Modification of the Surface Seawater Carbonate System

$p\mathrm{CO}_{2sw}$ is ultimately controlled by the equilibrium condition of the seawater carbonate system. DIC, TA, salinity and water temperature all affect this equilibrium, and thus exert a control on $p\mathrm{CO}_{2sw}$. In terms of gas exchange, it is actually the carbonate system properties of the very thin mass diffusive layer that determines the air–sea $\Delta p\mathrm{CO}_2$.

The most obvious modification by lead formation is cooling of the sea surface, which will reduce $p\mathrm{CO}_{2sw}$ and increase solubility. Although the seawater will be near its freezing point, cooling beyond the freezing point (supercooling) occurs before ice formation begins. If no particles are available for the nucleation of ice crystals, supercooling can easily exceed 2° C [*Tsang and Hanley*, 1985]; a condition which can be created in the laboratory, but is not likely to exist in the Arctic. Observations of supercooling in the field are sparse, but *Skogseth et al.* [2009] observed a supercooling of ∼0.04 °C in the bulk surface water of an open coastal polynya in Svalbard. Given that the heat loss is at the surface, this would likely translate into an even more significant cooling of the diffusive mass boundary layer – in essence, the rapid sensible heat flux would drive a very pronounced cool–skin effect.

This cool–skin effect would enhance uptake when the sea surface was undersaturated due to increased solubility and decreased $p\mathrm{CO}_{2sw}$, but would actually act to restrict exchange when the surface was supersaturated. Given that we measured one instance of intense outgassing (case 3, section 4.1.2), this process alone cannot account for the high exchange rates.

Frazil ice formation and the accompanying rejection of brines also has the potential to modify the near–surface chemistry. A decrease in solubility driven by salt rejection and rising DIC/TA concentrations may either suppress or enhance gas exchange, depending on the saturation state. When the sea surface is supersaturated, the added DIC/TA and reduced solubility should enhance outgassing. When the sea surface is undersaturated, these combined effects should suppress uptake. However, whether or not this has an influence on gas exchange depends on where the brines ultimately end up. On the nearby Beaufort Sea Shelf, *Melling and Moore* [1995] showed that deep penetration to the pycnocline of brine does occur at times, which suggests that modification of the near–surface chemistry may not be important. *Shadwick et al.* [2011] did measure long–term surface increases in salinity, and DIC/TA in Amundsen Gulf over the winter, but we do not have measurements that capture the evolution of these properties on the timescale of an individual flaw lead event. On these short timescales, we hypothesize that the effects of brine rejection will be minor. Since most of the frazil ice formation is occurring below the ocean skin, there will not be much immediate modification of the chemistry of the mass diffusive layer. *Ushio and Wakatsuchi* [1993] also showed that the brine rejection from frazil crystals is concentrated in thin streamers that rapidly descend downwards. If leads are small and short-lived, there would be a significant amount of unmodified water available laterally and vertically to replace those descending brines, keeping the surface water properties near–constant.

Ultimately, we cannot draw any firm conclusions regarding the short timescale modifications to the seawater carbonate system. However, given the manner in which the carbonate system is entwined with many of the processes that occur with lead formation, this should be a major focus of future studies.

5.3. Significance to the Amundsen Gulf Region

The total winter CO_2 flux through open water in the Amundsen Gulf depends on not only the rate at which it occurs, but also on the areal extent of open water. In this section, we combine estimates of these two variables for the purpose of computing area–averaged fluxes. By calculating these fluxes, we can estimate the significance of winter CO_2 exchange relative to the open water season (i.e. late spring/summer/early fall), and we can determine if the fluxes are reasonable based on the water column DIC budget for the region devised by *Shadwick et al.* [2011].

As described in section 3.5, we used RADARSAT–1 imagery to estimate the open water fraction in a bounding box (122–126°W, 70–71.5°N) consistent with the one used by *Shadwick et al.* [2011]. RADARSAT–1 images that captured this area were available approximately every week, and the open water fraction calculated for each image are shown in Figure 13. The amount of open water during the study was highly variable, which probably relates to storm events in the area. To allow comparisons with the results of *Shadwick et al.* [2011], monthly averages of open water fraction were calculated, and are displayed in Table 3.

To estimate the rate of gas exchange over the area we would ideally have some way of scaling our flux measurements using $\Delta p\mathrm{CO}_2$ and an easily-obtainable variable like wind speed, but at this point our dataset is too limited to work towards parameterization. Therefore, we simply calculated the mean uptake rate from cases 1,4,7 & 17 (those with substantial uptake; the outgassing observed during case 3 was omitted because the offshore Amundsen Gulf was undersaturated through the entire winter [*Shadwick et al.*, 2011]) to be -4.88 μmol m^{-2} s^{-1}. This rate was multiplied by the average monthly open water fraction to calculate the mean monthly fluxes shown in Table 3.

To address the question of whether these fluxes are reasonable we integrated the flux over each month, and calculated the net change in DIC (denoted $\Delta\mathrm{DIC}_{as-enh}$ in Table 3) that would occur assuming a 50m mixed–layer depth. *Shadwick et al.* [2011] budgeted month-by-month changes in DIC in the Amundsen Gulf mixed layer via:

$$\Delta\mathrm{DIC}_{obs} = \Delta\mathrm{DIC}_{bio} + \Delta\mathrm{DIC}_{fw} + \Delta\mathrm{DIC}_{as} + \Delta\mathrm{DIC}_{vd} \tag{3}$$

where $\Delta\mathrm{DIC}_{obs}$ was the observed monthly change in DIC, and the right hand terms are monthly changes in DIC due to biological activity ($\Delta\mathrm{DIC}_{bio}$), freshwater fluxes ($\Delta\mathrm{DIC}_{fw}$), air–sea exchange ($\Delta\mathrm{DIC}_{as}$) and vertical diffusion ($\Delta\mathrm{DIC}_{vd}$). $\Delta\mathrm{DIC}_{fw}$ and $\Delta\mathrm{DIC}_{vd}$ were calculated from in situ data, and $\Delta\mathrm{DIC}_{as}$ was calculated using a bulk flux approach scaled for ice concentration. No direct method was available to measure the biological contribution, so it was calculated as a difference of the 4 other terms. With no other constraint on the biological contribution to $\Delta\mathrm{DIC}_{obs}$, a flux of CO_2 which is enhanced beyond $\Delta\mathrm{DIC}_{as}$ would be mis-allocated into $\Delta\mathrm{DIC}_{bio}$. Thus if our calculated $\Delta\mathrm{DIC}_{as-enh}$ fits within the sum of $\Delta\mathrm{DIC}_{as}$ and $\Delta\mathrm{DIC}_{bio}$ it can be considered to fit in the budget.

Table 3 shows that this is the case in all months under consideration, except November. This shows that although the fluxes associated with this enhanced air–sea exchange are very high, they are not unrealistic from the standpoint of the DIC budget.

With respect to significance for the Amundsen Gulf region, the fluxes calculated accounting for enhanced air–sea exchange are more than an order of magnitude higher than those calculated by *Shadwick et al.* [2011] using a bulk flux approach scaled for ice concentration (Table 3). In fact, these fluxes place the air–sea exchange rates on par with the open water season rates calculated by *Shadwick et al.* [2011]. This is a significant consideration, because the typical model of a polynya's annual air–sea budget is characterized by open water uptake during the autumn storm season (utilizing an initial biological $p\mathrm{CO}_{2sw}$ drawdown in the spring) which is then capped by ice over the winter [*Yager et al.*, 1995]. The strength of annual uptake by a polynya was thought to be constrained by whether or not the spring undersaturation could be utilized by open water air–sea exchange, but the results from this study show that uptake may proceed beyond ice formation. It should be noted, however, that not every polynya may remain undersaturated through the winter; in polynyas where this is not the case, winter outgassing through open water may tip the annual balance away from net uptake.

5.4. Potential Significance to the Arctic Ocean

As well as creating a need to re-think the seasonal evolution of gas exchange for polynyas, enhanced winter gas exchange may play an important role in the broader Arctic and Antarctic Oceans. *Omar et al.* [2005] used a simple extrapolation of winter air–sea CO_2 exchange estimated in Storfjorden to show that Arctic polynyas are likely a significant sink for atmospheric CO_2. Our study confirms that at least one other Arctic polynya behaves as they predict, an important step in validating their larger scale estimates. In addition to polynyas, we hypothesize that flaw leads may act as important centres for winter gas exchange. Leads are typically a small fraction of the Arctic icescape during winter; *Lindsay and Rothrock* [1995] estimated the percentage to be 2–3% for the central Arctic and 6–9% for the peripheral seas. However, our findings suggest that even at low fractions these features may dominate the winter gas exchange budget much in the same way that they dominate heat fluxes [*Maykut*, 1978; *Andreas*, 1980]. Also of note are the large areas of the Arctic and Antarctic ocean which are seasonally ice-free. In the Arctic, this makes up an area of 6.4×10^6 km^2 and in the Antarctic 15.2×10^6 km^2 (*Wadhams* [2000], 1979-87 averages). As discussed by *Omar et al.* [2005], the seasonal formation of sea ice over these areas may create short but intense CO_2 fluxes which could be important to the annual air-sea CO_2 exchange budget of the Arctic and Southern Oceans.

Ongoing and anticipated changes in the polar oceans may further increase the importance of this effect. The rapidly decreasing summer ice extent in the Arctic (e.g. *Stroeve et al.* [2007]) means that a larger area will be subject to annual ice formation, and significant positive trends in sea ice motion [*Hakkinen et al.*, 2008] may create more winter–time open water. Our results show that this will permit larger annual air–sea gas exchange, but whether this will result in a larger net sink of CO_2 is complicated. Surface seawater that is undersaturated in $p\mathrm{CO}_{2sw}$ can only absorb a finite amount of CO_2, depending on the state of the carbonate equilibrium (i.e. the Revelle factor). A debate is currently emerging regarding whether the ocean surface exposed by recent sea ice loss has the capacity to take up significant amounts of CO_2 [*Bates*, 2006; *Cai et al.*, 2010]. A similar debate needs to be had regarding uptake capacity of the Arctic Ocean at freeze–up in order to understand the potential for gas exchange enhanced by ice formation. A net annual sink also requires export of absorbed CO_2 to depth, a process that appears to occur effectively on the shelves where deep water formation occurs but not necessarily in the Arctic Ocean basins [*Omar et al.*, 2005]. Clearly, a lot of work remains to be done before we can fully understand the interplay between enhanced gas exchange and future changes to the Arctic Ocean.

6. Summary and Conclusions

This paper has provided the first direct, in situ observations of enhanced gas exchange during sea ice formation. Eddy covariance calculations of CO_2 flux in Amundsen Gulf (a polynya with a dynamic winter sea ice cover) showed periods of intense uptake (mean flux -4.88, maximum -27.95 μmol m^{-2} s^{-1}) and one case of outgassing (mean flux +2.10 μmol m^{-2} s^{-1}). These periods of high gas exchange were observed coincidentally with high heat fluxes, which we confirmed from satellite imagery to be the result of open water (i.e. flaw leads). Conversely, we measured no fluxes above the uncertainty of our instruments over consolidated sea ice.

We presented several hypotheses to explain our observations of enhanced gas transfer. In a winter flaw lead, we expect high water–side turbulence to occur as a result of rapid heat loss and salt rejection. Since turbulence is the first–order control on gas exchange, we hypothesize that this high turbulence is a major cause of enhanced gas exchange. We also discussed the modification of surface properties (temperature, salinity, DIC/TA) and their effect on the seawater carbonate system. The potential of these modifications to influence the rate of gas exchange depends on the saturation state of CO_2 with respect to the atmosphere, and at times may actually be contradictory to high fluxes. In support of these hyptoheses, we were only able to provide limited evidence of high turbulence in the region.

By comparing our flux values with DIC measurements we were able to show that although high, they do fit within surface DIC budgets. A rough calculation of the integrated CO_2 uptake over the months of Nov.–Jan. showed that winter gas exchange may in fact be as important as the open water (i.e. late spring/summer/early fall) seasons. These results have wide reaching implications for understanding the annual air–sea CO_2 budgets of polynyas and other seasonally ice–free seas.

Acknowledgments.

Thank you to the Captains and crew of the *CCGSAmundsen* and the many people who helped in the field: Bruce Johnson, Sarah Woods, Kyle Swystun, Gauthier Carnat, Elizabeth Shadwick, Keith Johnson, Jens Ehn, Silvia Gremes-Cordero, Sylvain Blondeau, Luc Michaud and many others. Thank you to John Prytherch, whose help with the PKT correction is greatly appreciated. We also acknowledge the thoughtful input of two anonymous reviewers who greatly improved the manuscript. This work is a contribution to the International Polar Year-Circumpolar Flaw Lead System Study (IPY-CFL 2008), supported by the Canadian IPY Federal program office, the Natural Sciences and Engineering Research Council (NSERC) and many other contributors. The authors of this paper are members of ArcticNet, funded in part by the Networks of Centres of Excellence Canada, NSERC, the Canadian Institute of Health Research and the Social Sciences and Humanities Research Council. B. Else is supported by a Vanier Canada Graduate Scholarship, and received funding for logistics from the Northern Scientific Training Program.

We gratefully acknowledge the continued support of the Centre for Earth Observation Science and the University of Manitoba.

References

Amiro, B. (2010). Estimating annual carbon dioxide eddy fluxes using open-path analysers for cold forest sites. *Agricultural and Forest Meteorology*, 150(10):1366–1372, doi:10.1016/j.agrformet.2010.06.007.

Anctil, F., Donelan, M.A., Drennan, W.M., and Graber, H.C. (1994). Eddy-correlation measurements of air-sea fluxes from a discus buoy. *Journal of Atmospheric and Oceanic Technology*, 11:1144–1150.

Anderson, L.G., Falck, E., Jones, E.P., Jutterström, S., and Swift, J.H. (2004). Enhanced uptake of atmospheric CO_2 during freezing of seawater: A field study in Storfjorden, Svalbard. *Journal of Geophysical Research*, 109 (C06004), doi:10.1029/2003JC002120.

Andreas, E.L. (1980). Estimation of heat and mass fluxes over arctic leads. *Monthly Weather Review*, 108:2957–2063.

Asher, W.E., Karle, L.M., Higgins, B.J., Farley, P.J., Monahan, E.C., and Leifer, I.S. (1996). The influence of bubble plumes on air-seawater gas transfer velocities. *Journal of Geophysical Research*, 101(C5):12,027-12,041, doi:10.1029/96JC00121.

Bates, N., Moran, S., Hansell, D., and Mathis, J. (2006). An increasing CO_2 sink in the Arctic Ocean due to sea–ice loss. *Geophysical Research Letters*, 33:L23609

Bock, E.J., Hara, T., Frew, N.M., and McGillis, W.R. (1999). Relationship between air sea gas transfer and short wind waves. *Journal of Geophysical Research*, 104(C11):25,821-25,831, doi:10.1029/1999JC900200.

Bolin, B. (1960). On the exchange of carbon dioxide between the atmosphere and the sea. *Tellus*, 12(3):274–281.

Bourgault, D., Kelley, D.E., and Galbraith, P.S. (2008). Turbulence and boluses on an internal beach. *Journal of Marine Research*, 66:563–588.

Burba, G.G., McDermitt, D.K., Grelle, A.G., Anderson, D.J., and Xu, L. (2008). Addressing the influence of instrument surface heat exchange on the measurements of CO_2 flux from open-path gas analyzers. *Global Change Biology*, 14(8):1854–1876, doi: 10.1111/j.1365-2486.2008.01606.x.

Cai, W., Chen, L., Chen, B., Gao, Z., Lee, S., Chen, J., Pierrot, D., Sullivan, K., Wang, Y., Hu, X., et al. (2010). Decrease in the CO_2 uptake capacity in an ice-free Arctic Ocean basin. *Science*, 329(5991):556.

Denman, K., Brasseur, G., Chidthaisong, A., Ciais, P., Cox, P., Dickinson, R., Hauglustaine, D., Heinze, C., Holland, E., Jacob, D., Lohmann, U., Ramachandran, S., da Silva Dias, P., Wofsy, S., and Zhang, X. (2007). Couplings between changes in the climate system and biogeochemistry. In Solomon, S., Qin, D., Manning, M., Marquis, M., Averyt, K., Tignor, M., and Miller, H., editors, *Climate change 2007: The Physical Science Basis. Contribution of Working Group I to the Fourth Assessment Report of the Intergovernmental Panel on Climate Change*, chapter 7. Cambridge University Press, United Kingdom and New York, NY, USA.

Dugan, J.P., Panichas, S.L., and DiMarco, R.L. (1991). Decontamination of wind measurements from buoys subjected to motions in a seaway. *Journal of Atmospheric and Oceanic Technology*, 8:85–95.

Edson, J.B., Hinton, A.A., Prada, K.E., Hare, J.E., and Fairall, C.W. (1998). Direct covariance flux estimates from mobile platforms at sea. *Journal of Atmospheric and Oceanic Technology*, 15:547–562, doi: 10.1175/1520-0426(1998)015.

Frew, N.M. (1997). The role of organic films in air-sea gas exchange. In *The Sea Surface and Global Change*, edited by P.S. Liss, R.A. Duce, *Cambridge University Press*, 121–173.

Frew, N.M., Bock, E.J., Schimpf, U., Hara, T., Haußecker, H., Edson, J.B., McGillis, W.R., Nelson, R.K., McKenna, S.P., Uz, B.M., Jähne, B. (2004). Air-sea gas transfer: Its dependence on wind stress, small-scale roughness, and surface films. *Journal of Geophysical Research*, 109(C8):C08S17, doi:10.1029/2003JC002131.

Fujitani, T. (1981). Direct measurement of turbulent fluxes over the sea during AMTEX. *Papers in Meteorology and Geophysics*, 32(3):119–134.

Galley, R.J., Key, E., Barber, D.G., Hwang, B.J., and Ehn, J.K. (2008). Spatial and temporal variability of sea ice in the southern Beaufort Sea and Amundsen Gulf: 1980–2004. *Journal of Geophysical Research*, 113(C5):C05S95, doi:10.1029/2007JC004553.

Golden, K., Ackley, S., and Lytle, V. (1998). The percolation phase transition in sea ice. *Science*, 282(5397):2238–2241.

Gosink, T.A., Pearson, J.G., and Kelley, J.J. (1976). Gas movement through sea ice. *Nature*, 263:41–42, doi:10.1038/263041a0.

Hakkinen, S., Proshutinsky, A., and Ashik, I. (2008). Sea ice drift in the Arctic since the 1950s. *Geophysical Research Letters*, 35:L19704, doi:10.1029/2008GL034791.

Hirata, R., Hirano, T., Saigusa, N., Fujinuma, Y., Inukai, K., Kitamori, Y., Takahashi, Y., and Yamamoto, S. (2007). Seasonal and interannual variations in carbon dioxide exchange of a temperate larch forest. *Agricultural and Forest Meteorology*, 147(3-4):110–124, doi:10.1016/j.agrformet.2007.07.005.

Ho, D.T., Law, C.S., Smith, M.J., Schlosser, P., Harvey, M., and Hill, P. (2006). Measurements of air-sea gas exchange at high wind speeds in the Southern Ocean: Implications for global parameterizations. *Geophysical Research Letters*, 33:L23503, doi:10.1029/2006GL026817.

Ho, D.T., Zappa, C.J., McGillis, W.R., Bliven, L.F., Ward, B., Dacey, J.W., Schlosser, P., and Hendricks, M.B. (2004). Influence of rain on air-sea gas exchange: Lessons from a model ocean. *Journal of Geophysical Research*, 109:C08S18, doi:10.1029/2003JC001806.

Jähne, B. (1987). On the parameters influencing air-water gas exchange. *Journal of Geophysical Research*, 92(C2):1937–1950, 10.1029/JC092iC02p01937.

Järvi, L., Mammarella, I., Eugster, W., Ibrom, A., Siivola, E., Dellwik, E., Keronen, P., Burba, G., and Vesala, T. (2009). Comparison of net CO_2 fluxes measured with open-and closed-path infrared gas analyzers in an urban complex environment. *Boreal Environment Research*, 14:499–514.

Kaimal, J.C. and Gaynor, J.E. (1991). Another look at sonic thermometry. *Boundary-Layer Meteorology*, 56:401–410.

Kohsiek, W. (2000). Water vapor cross-sensitivity of open path H_2O/CO_2 sensors. *Journal of Atmospheric and Oceanic Technology*, 17:299–311.

Körtzinger, A., Thomas, H., Schneider, B., Gronau, N., Mintrop, L., and Duinker, J.C. (1996). At-sea intercomparison of two newly designed underway pCO$_2$ systems–encouraging results. *Marine Chemistry*, 52(2):133–145, doi:10.1016/0304-4203(95)00083-6.

Kuss, J. and Schneider, B. (2004). Chemical enhancement of the CO_2 gas exchange at a smooth seawater surface. *Marine Chemistry*, 91(1-4):165–174, doi:10.1016/j.marchem.2004.06.007.

Leuning, R. (2004). Measurements of trace gas fluxes in the atmosphere using eddy covariance: WPL corrections revisited. In *Handbook of micrometeorology: A guide to surface flux measurement and analysis*, edited by Lee X., Massman W.J., Law B.E. , *Boston:Kluwer*, 119–32.

Lindsay, R.W. and Rothrock, D.A. (1995). Arctic sea ice leads from advanced very high resolution radiometer images. *Journal of Geophysical Research*, 100(C3):4533–4544, doi:10.1029/94JC02393.

Liss, P.S. and Merlivat, L.. (1986). Air-sea gas exchange rates: Introduction and synthesis. In *The role of air–sea exchange in geochemical cycling*, edited by Buat-Menard, P. , *Boston:D. Reidel Publishing Company*, 113-127

Loose, B., McGillis, W.R., Schlosser, P., Perovich, D., and Takahashi, T. (2009). Effects of freezing, growth, and ice cover on gas transport processes in laboratory seawater experiments. *Geophysical Research Letters*, 36(5):L05603, doi:10.1029/2008GL036318.

Loose, B., Schlosser, P., Perovich, D., Ringelberg, D., Ho, D., Takahashi, T., Richter-Menge, J., Reynolds, C., McGillis, W., and Tison, J.-L. (2010). Gas diffusion through columnar laborator sea ice: implications for mixed layer ventilation of co_2 in the seasonal sea ice zone. *Tellus B*, pages doi: 10.1111/j.1600–0889.2010.00506.x.

Maykut, G.A. (1978). Energy exchange over young sea ice in the Central Arctic. *Journal of Geophysical Research*, 83(C7):3646–3658, doi:10.1029/JC083iC07p03646.

McGillis, W.M., Edson, J.B., Ware, J.E., Dacey, J.H.W., Hare, J.E., Fairall, C.W., and Wanninkhof, R. (2001). Carbon dioxide flux techniques performed during GasEx-98. *Marine Chemistry*, 75:267–280, doi:10.1016/S0304-4203(01)00042-1.

McGillis, W.R., Edson, J.B., Zappa, C.J., Ware, J.D., McKenna, S.P., Terray, E.A., Hare, J.E., Fairall, C.W., Drennan, W.M., Donelan, M., DeGrandpre, M.D., Wanninkhof, R., and Feely, R.A. (2004). Air-sea CO_2 exchange in the equatorial Pacific. *Journal of Geophysical Research*, 109:C08S02, doi:10.1029/2003JC002256.

McPhee, M.G. and Stanton, T.P. (1996). Turbulence in the statically unstable oceanic boundary layer under arctic leads. *Journal of Geophysical Research*, 101(C3):6409–6428.

Melling, H. and Moore, R. (1995). Modification of halocline source waters during freezing on the Beaufort Sea shelf: evidence from oxygen isotopes and dissolved nutrients. *Continental Shelf Research*, 15(1):89–113.

Mitsuta, Y. and Fujitani, T. (1974). Direct measurement of turbulent fluxes on a cruising ship. *Boundary-Layer Meteorology*, 6:203–217, doi: 10.1007/BF00232485.

Mucci, A., Lansard, B., Miller, L.A., and Papakyriakou, T.N. (2010). CO_2 fluxes across the air–sea interface in the southeastern Beaufort Sea: Ice–free period. *Journal of Geophysical Research*, 115(C04003), doi:10.1029/2009JC005330.

Murata, A. and Takizawa, T. (2003). Summertime CO_2 sinks in shelf and slope waters of the western Arctic Ocean. *Continental Shelf Research*, 23(8):753–776, doi:10.1016/S0278-4343(03)00046-3.

Nightingale, P.D., Malin, G., Law, C.S., Watson, A.J., Liss, P.S., Liddicoat, M.I., Boutin, J., and Upstill-Goddard, R.C. (2000). In situ evaluation of air-sea gas exchange parameterizations using novel conservative and volatile tracers. *Global Biogeochemical Cycles*, 14:373–387, doi:10.1029/1999GB900091.

Nomura, D., Yoshikawa-Inoue, H., and Toyota, T. (2006). The effect of sea-ice growth on air–sea co_2 flux in a tank experiment. *Tellus B*, 58(5):418–426.

Omar, A., Johannessen, T., Bellergy, R.G.J., Olsen, A., Anderson, L.G., and Kivimäe (2005). Sea–ice and brine formation in Storfjorden: Implications for the Arctic wintertime air–sea CO_2 flux. In *The Nordic Seas: an Integrated Perspective*, edited by H. Drange, T. Dokken, T. Furevik, R. Gerdes, W. Berger, *American Geophysical Union, Geophysical Monograph 158*, 177–189.

Omstedt, A. (1985). On supercooling and ice formation in turbulent sea-water. *Journal of Glaciology*, 31:263–271.

Ono, K., Miyata, A., and Yamada, T. (2008). Apparent downward CO_2 flux observed with open-path eddy covariance over a non-vegetated surface. *Theoretical and Applied Climatology*, 92(3):195–208, doi: 10.1007/s00704-007-0323-3.

Prytherch, J., Yelland, M.J., Pascal, R.W., Moat, B.I., Skjelvan, I., and Neill, C.C. (2010). Direct measurements of the CO_2 flux over the ocean: Development of a novel method. *Geophysical Research Letters*, 37(3):L03607, doi:10.1029/2009GL041482.

Rysgaard, S., Glud, R.N., Sejr, M.K., Bendtsen, J., and Christensen, P.B. (2007). Inorganic carbon transport during sea ice growth and decay: A carbon pump in polar seas. *Journal of Geophysical Research*, 112:C03016, doi:10.1029/2006JC003572.

Rysgaard, S., Bendtsen, J., Pedersen, L.T., Ramløv, H., Glud, R.N. (2009). Increased CO_2 uptake due to sea ice growth and decay in the Nordic Seas. *Journal of Geophysical Research*, 114:C09011, doi:10.1029/2008JC005088.

Shadwick, E., Thomas, H., Chierici, M., Else, B., Fransson, A., Michel, C., Miller, L., Mucci, A., Niemi, A., Papakyriakou, T., and J.-É., T. (2011). Seasonal variability of the inorganic carbon system in the Amundsen Gulf region of the southeastern Beaufort Sea. *Limnology and Oceanography*, 56(1), 303–322, doi:10.4319/lo.2011.56.1.0303.

Skogseth, R., Nilsen, F., and Smedsrud, L.H. (2009). Supercooled water in an Arctic polynya: observations and modeling. *Journal of Glaciology*, 55(189):43–52.

Stroeve, J., Holland, M.M., Meier, W., Scambos, T., and Serreze, M. (2007). Arctic sea ice decline: Faster than forecast. *Geophysical Research Letters*, 34(9):9501, doi:10.1029/2007GL029703.

Sweeney, C., Gloor, E., Jacobson, A.R., Key, R.M., McKinley, G., Sarmiento, J.L., and Wanninkhof, R. (2007). Constraining global air-sea gas exchange for CO_2 with recent bomb ^{14}C measurements. *Global Biogeochemical Cycles*, 7:843–878, doi:10.1029/2006GB002784.

Takagaki, N. and Komori, S. (2007). Effects of rainfall on mass transfer across the air-water interface. *Journal of Geophysical Research*, 112(C6):C06006, doi:10.1029/2006JC003752.

Takahashi, T., Olafsson, J., Goddard, J.G., Chipman, D.W., and Sutherland, S.C. (1993). Seasonal variation of CO_2 and nutrients in the high-latitude surface oceans: a comparative study. *Global Biogeochemical Cycles*, 7(4):843–878, doi:10.1029/93GB02263.

Takahashi, T., Sutherland, S.C., Wanninkhof, R., Sweeney, C., Feely, R.A., Chipman, D.W., Hales, B., Friederich, G., Chavez, F., Sabine, C., et al. (2009). Climatological mean and decadal change in surface ocean $p\mathrm{CO}_2$, and net sea-air CO_2 flux over the global oceans. *Deep Sea Research Part II: Topical Studies in Oceanography*, 56(8-10):554–577, doi:10.1016/j.dsr2.2008.12.009 .

Tsang, G. and Hanley, T. O'D. (1985). Frazil formation in water of different salinities and supercoolings. *Journal of Glaciology*, 31(108).

Ushio, S. and Wakatsuchi, M. (1993). A laboratory study on supercooling and frazil ice production processes in winter coastal polynyas. *Journal of Geophysical Research*, 98(C11):20321.

Wadhams, P. (2000). Ice in the Ocean. *Gordon and Breach Science Publishers*

Wanninkhof, R. (1992). Relationship between wind speed and gas exchange over the ocean. *Journal of Geophysical Research*, 97(C5):7373–7382.

Wanninkhof, R., Asher, W.E., Ho, D.T., Sweeney, C., and McGillis, W.R. (2009). Advances in quantifying air-sea gas exchange and environmental forcing. *Annual Review of Marine Science*, 1:213–244.

Wanninkhof, R. and McGillis, W.R. (1999). A cubic relationship between gas exchange and wind speed over the ocean. *Geophysical Research Letters*, 26:7373–7381, doi:10.1029/1999GL900363.

Webb, E.K., Pearman, G.I., and Leuning, R. (1980). Correction of flux measurements for density effects due to heat and water vapour transfer. *Quarterly Journal of the Royal Meteorological Society*, 106(447):85–100, doi: 10.1002/qj.49710644707.

Woolf, D.K. (1997). Bubbles and their role in gas exchange. In *The Sea Surface and Global Change*, edited by P.S. Liss, R.A. Duce, *Cambridge University Press*, 173–207.

Woolf, D.K. (2005). Parametrization of gas transfer velocities and sea-state-dependent wave breaking. *Tellus B*, 57(2):87–94, doi: 10.1111/j.1600-0889.2005.00139.x.

Woolf, D.K., Leifer, I.S., Nightingale, P.D., Rhee, T.S., Bowyer, P., Caulliez, G., De Leeuw, G., Larsen, S.E., Liddicoat, M., Baker, J., and Andreae, M.O. (2007). Modelling of bubble-mediated gas transfer: Fundamental principles and a laboratory test. *Journal of Marine Systems*, 66(1-4):71–91, doi:10.1016/j.jmarsys.2006.02.011.

Yager, P.L., Wallace, D.W.R., Johnson, K.M., Smith Jr., W.O., Minnett, P.J., Deming, J.W. (1995). The Northeast Water Polynya as an atmospheric CO_2 sink: A seasonal rectification hypothesis. *Journal of Geophysical Research*, 100(C3):4389–4398, doi:10.1029/94JC01962.

Zappa, C.J., Asher, W.E., Jessup, A.T., Klinke, J., and Long, S.R. (2004). Microbreaking and the enhancement of air-water transfer velocity. *Journal of Geophysical Research*, 109(C08S16):21, doi:10.1029/2003JC001897.

Zappa, C.J., Ho, D.T., McGillis, W.R., Banner, M.L., Dacey, J.W.H., Bliven, L.F., Ma, B., and Nystuen, J. (2009). Rain-induced turbulence and air-sea gas transfer. *Journal of Geophysical Research*, 114(C07009), doi:10.1029/2008JC005008.

Zappa, C.J., McGillis, W.R., Raymond, P.A., Edson, J.B., Hintsa, E.J., Zemmelink, H.J., Dacey, J.W.H., and Ho, D.T. (2007). Environmental turbulent mixing controls on air-water gas exchange in marine and aquatic systems. *Geophysical Research Letters*, 34(10):10601, doi:10.1029/2006GL028790.

Table 1. Summary of conditions experienced during each sample case

Table 2. Noise and bias in the eddy covariance system, including the effect of various corrections. Bias is calculated as the mean CO_2 flux from cases where near–zero flux is expected, noise is one standard deviation around that mean. The number of eddy covariance sample runs is 274 for raw and sensor heating corrected, 151 for crosstalk corrected.

Table 3. Summary of monthly lead fraction, CO_2 fluxes and resulting change in mixed layer DIC

Figure 1. Map of the Banks Island flaw lead/polynya complex. The light grey line shows the ship track. The shaded grey area represents the region which usually remains mobile through the time period under consideration, and the dotted line shows the areas typically associated with the Cape Bathurst polynya and flaw lead.

Figure 2. Measured CO_2 fluxes (including sensor heating correction) for the study period. The numbers along the top axis indicate the sample cases, the most interesting of which are discussed in the text, with the red brackets denoting their time frame. The inset shows observations made between Dec. 1–2 with an extended scale on the y-axis. The horizontal grey lines show the estimated noise level of the eddy covariance system as discussed in section 5.1

Figure 3. RADARSAT-1 image collected on Nov. 2 at 01:53, just prior to sample case 1. The inset map shows the location of the imaged area, red lines indicate the ship's track, the green X indicates the location of the ship at the time of image acquisition, and the green arrow shows the mean wind direction.

Figure 4. Time series of atmospheric measurements made during sample case 1. (a) Measured CO_2 flux with sensor heating correction added (open circles), and the estimated noise level of the system as discussed in section 5.1 (horizontal grey lines), (b) measured sensible heat flux (red open circles) and latent heat flux (blue open circles), (c) 1 minute averages of air temperature (dashed line) and wind velocity (solid line).

Figure 5. RADARSAT-1 image collected on Nov. 20 at 01:29, just prior to cases 3 and 4. The inset map shows the location of the imaged area, red lines indicate the ship's track, the green X indicates the location of the ship at the time of image acquisition, and the green arrow shows the mean wind direction.

Figure 6. Time series of atmospheric measurements made during sample cases 3 and 4 (division between the two cases is denoted by the dashed vertical line). (a) Measured CO_2 flux with sensor heating correction added (open circles), range of bulk CO_2 flux estimates (brackets), and the estimated detection limit of the system as discussed in section 4.2 (horizontal grey lines), (b) measured sensible heat flux (red open circles) and latent heat flux (blue open circles), (c) 1 minute averages of air temperature (dashed line) and wind velocity (solid line).

Figure 7. RADARSAT-1 image collected on Dec. 1, 14:45, just after case 7. The inset map shows the location of the imaged area, red lines indicate the ship's track, the green X indicates the location of the ship at the time of image acquisition, and the green arrow shows the mean wind direction.

Figure 8. Time series of atmospheric measurements made during sample case 7. (a) Measured CO_2 flux with sensor heating correction added (open circles), and the estimated noise level of the system as discussed in section 5.1 (horizontal grey lines), (b) measured sensible heat flux (red open circles) and latent heat flux (blue open circles), (c) 1 minute averages of air temperature (dashed line) and wind velocity (solid line).

Figure 9. RADARSAT-1 image collected on Jan. 24, 01:33, just prior to case 17. The inset map shows the location of the imaged area, red lines indicate the ship's track, the green X indicates the location of the ship at the time of image acquisition, and the green arrow shows the mean wind direction.

Figure 10. Time series of atmospheric measurements made during sample case 17. (a) Measured CO_2 flux with sensor heating correction added (open circles), and the estimated noise level of the system as discussed in section 5.1 (horizontal grey lines), (b) measured sensible heat flux (red open circles) and latent heat flux (blue open circles), (c) 1 minute averages of air temperature (dashed line) and wind velocity (solid line).

Figure 11. Time series of atmospheric measurements made during sample case 10. (a) Measured CO_2 flux with sensor heating correction added (open circles), and the estimated noise level of the system as discussed in section 5.1 (horizontal grey lines), (b) measured sensible heat flux (red open circles) and latent heat flux (blue open circles), (c) 1 minute averages of air temperature (dashed line) and wind velocity (solid line).

Figure 12. Schematic summarizing the important processes occurring during a wind–driven lead event. The processes highlighted in blue/red are those which likely have a direct effect on air–sea gas exchange. Processes in red are associated with frazil ice formation, and those in blue are associated with the surface cooling.

Figure 13. Open water percentage for Amundsen Gulf (122–126°W, 70–71.5°N) during the study period, as determined by classification of near-weekly RADARSAT-1 imagery.

Case	Date	Location (Lat/Lon)	CO_2 Flux (μmol m^{-2} s^{-1})	ΔCO_2 (μatm)	H Flux (W m^{-2})	E Flux (W m^{-2})	Air T (^oC)	Wind Vel. (m	Wind Dir. (deg)	Sea Ice Conditions
1	11/02 04:30-11/03 09:30	71.185[a] −129.096	-1.81	-80	43.3	4.1	-7.5	8.7	29	Newly forming grease ice
2	11/08 02:15-11/09 00:50	69.498 −123.930	0.23	146.5	7.3	3.7	-18.9	5.5	131.1	Newly forming fast ice. Estimated thickness: 30-40cm
3	11/20 01:30-11/20 14:45	71.038 −123.297	2.1	-77.4	53.8	9.9	-15.2	12.5	98.4	Mobile ice with upwind leads, thickness: 37cm
4	11/20 16:00-11/20 18:30	71.071 −123.430	-9.58	-66.7	111.4	11.3	-14.2	11.8	110.8	Mobile ice with upwind leads, thickness: 37cm
5	11/28 07:30-11/29 02:00	70.419[a] −126.372	0.55	15.8	-2.3	0.8	-16	8	254.6	Consolidated mobile ice, thickness: 52cm
6	11/30 05:15-11/30 23:30	71.053[a] −123.954	-0.03	-52.1	1.3	-1.1	-15.8	11.5	314.1	Consolidated, ridged ice floe

7	12/01 07:00-12/01 12:30	71.590[a] −124.656	-26.88	N/A	33.4	-10.4	-16.6	7.3	3.4	Transit through active lead with open water and grease ice
8	12/01 13:45-12/02 02:45	71.901 −125.441	0.31	-63.6	-2.9	0	-19.7	5.1	37.3	Land fast ice
9	12/02 05:30-12/02 22:15	71.725 −125.597	0.35	-69.4	1.3	-0.3	-18.2	3.4	47.1	Consolidated ice floe, thickness: 35cm
10	12/04 21:00-12/06 12:15	71.402[a] −124.875	-0.09	-86.7	15.8	2	-18	5.1	267.3	Consolidated ice floes, varying thicknesses: 25– 45cm
11	12/19 23:15-12/22 18:15	71.915 −125.433	0.42	-49.8	-0.6	3.3	-22	4.6	108.8	Land fast ice
12	12/24 20:45-12/25 17:15	71.262 −124.383	-0.14	-51	5.5	1.3	-20.7	5.9	123.2	Consolidated mobile ice, thickness: 30cm
13	01/02 18:15-01/06 03:30	71.306[a] −124.722	-0.5	-52	-7.9	5.3	-21.8	11.6	117.9	Thick consolidated ice floe, thickness: 105cm

14	01/10 09:15- 01/11 18:45	71.653[a] -126.101	0.58	-78.3	2.9	1.2	-21.3	7	123.3	Consolidated mobile ice
15	01/13 16:00- 01/14 22:00	71.494[a] -124.638	0.34	-73.8	3.2	1	-25	8	62.4	Consolidated mobile ice
16	01/20 17:00- 01/21 04:30	71.579 -125.104	0.34	N/A	-2.9	2.8	-18.9	6.4	123.6	Consolidated mobile ice, thickness: 91cm
17	01/24 08:00- 01/25 05:30	71.203 -125.184	-3.15	-38.4	16.4	5.6	-20.3	11. 9	291.7	Consolidated mobile ice, upwind leads
18	01/25 18:00- 01/26 16:30	71.172 -125.014	-0.86	-8.6	9.4	2	-25.7	8.7	298.5	Consolidated mobile ice
	[a]Ship was in transit, or drifting significantly: reported value is the midpoint of the sampling period									

	Bias (μmol m^{-2} s^{-1})	Noise (μmol m^{-2} s^{-1})
Raw (uncorrected)	-0.45	±0.76
Sensor heating corrected	0.13	±0.77
Water vapour crosstalk correction	-0.21	±1.32

	November	December	January
[a] Mean Open Water (%)	6.4	4.1	1.2
[b] $FCO2_{sw\text{-}mon}$ (μmol m^{-2} s^{-1})	-0.3	-0.2	-0.1
[c] $\Delta DIC_{as\text{-}enh}$ (μmol kg^{-1})	16.2	10.7	3.1
[d] ΔDIC_{as} (μmol kg^{-1}) [*Shadwick et al.,* 2011]	1	2	0.1
[e] ΔDICbio (μmol kg^{-1}) [*Shadwick et al.,* 2011]	3.0 ± 10.0	13.0 ± 10.0	16.0 ± 10.0

[a] Calculated from RADARSAT-1 image classification, [b] calculated from mean of cases 1,4,7 & 17, multiplied by lead fraction and integrated over the month, [c] calculated change in DIC concentration over a 50m mixed-layer using $FCO2_{sw\text{-}mon}$, [d] calculated change in DIC concentration over a 50 m mixed-layer using bulk-flux estimates scaled for open water fraction (from *Shadwick et al.* [2011]), [e] calculated change in DIC concentration over a 50m mixed layer due to biological activity (from *Shadwick et al.* [2011].

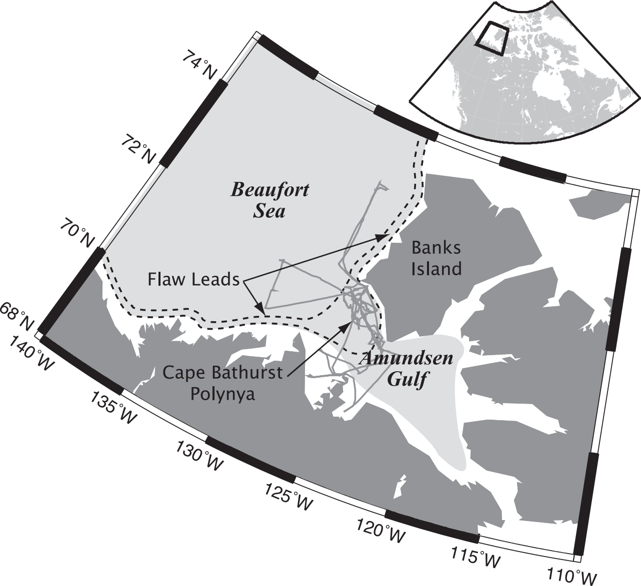

74°N
72°N
70°N
68°N
140°W
135°W
130°W
125°W
120°W
115°W
110°W
Beaufort Sea
Banks Island
Flaw Leads
Cape Bathurst Polynya
Amundsen Gulf

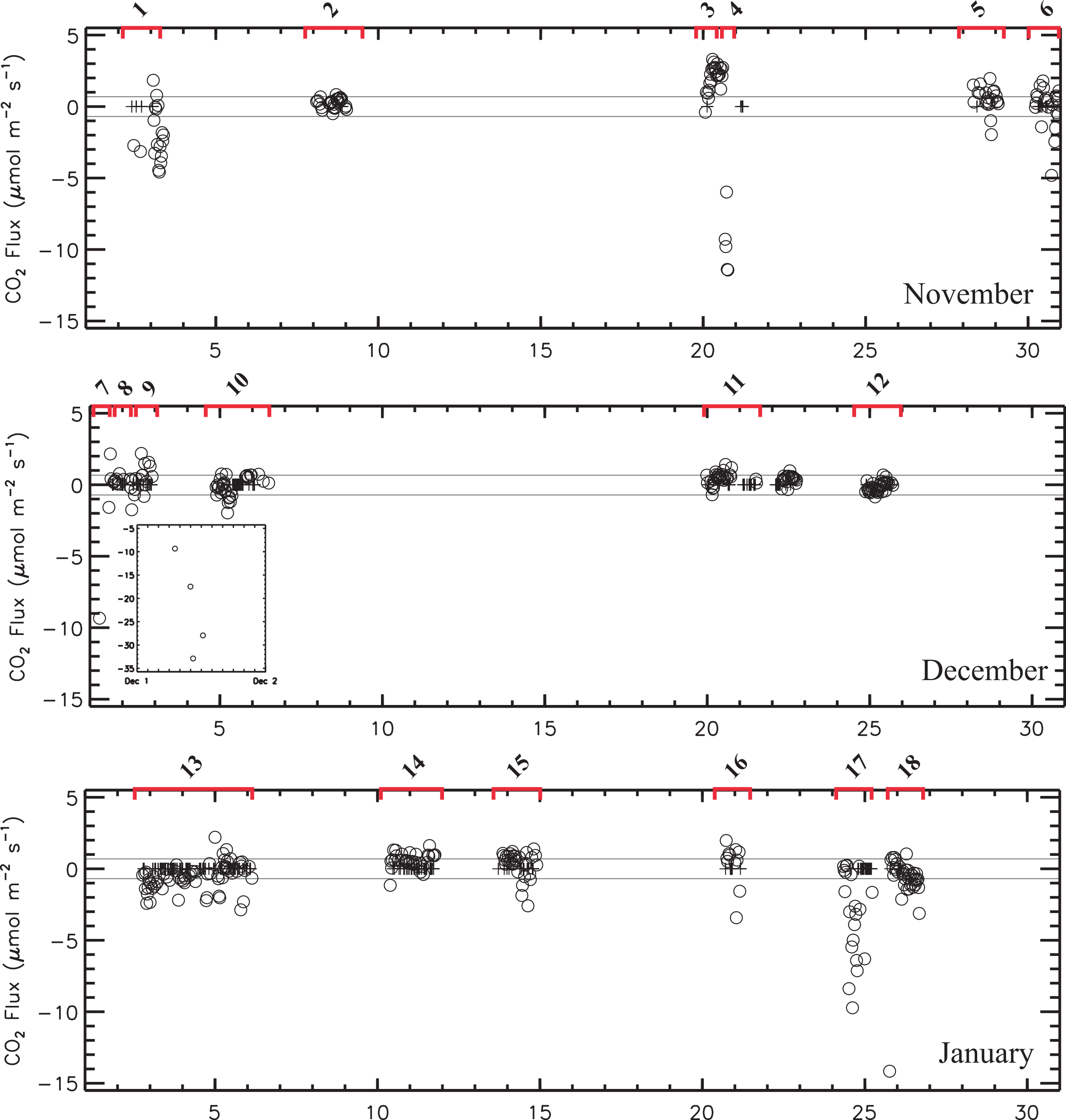

November
December
January
CO2 Flux (μmol m−2 s−1)
1
2
3
4
5
6
7
8
9
10
11
12
13
14
15
16
17
18
Dec 1
Dec 2

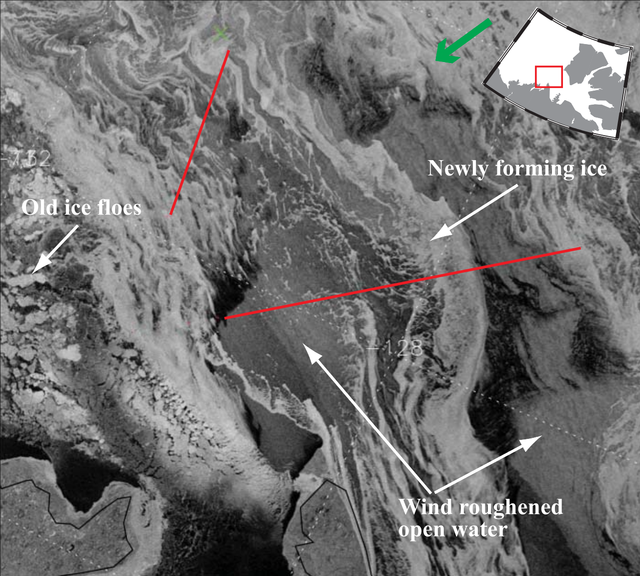

-7.52
Old ice floes
Newly forming ice
-128
Wind roughened
open water

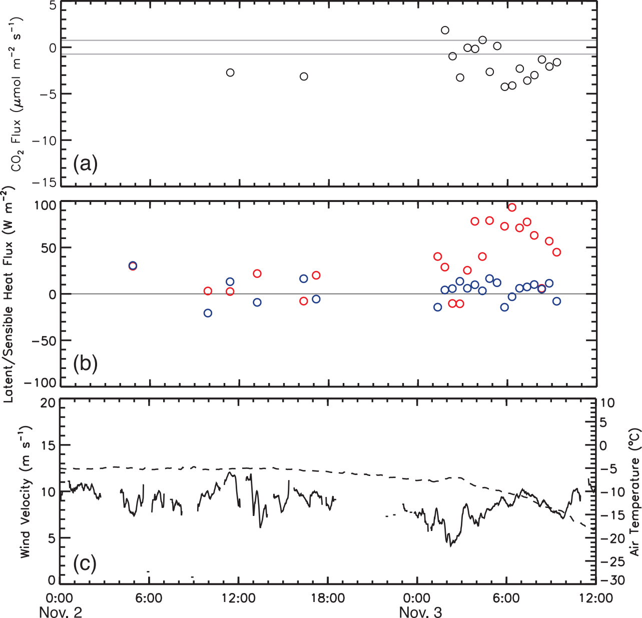

CO2 Flux (μmol m−2 s−1)
5
0
−5
−10
−15
(a)
Latent/Sensible Heat Flux (W m−2)
100
50
0
−50
−100
(b)
Wind Velocity (m s−1)
20
15
10
5
0
Air Temperature (°C)
10
5
0
−5
−10
−15
−20
−25
−30
(c)
0:00
Nov. 2
6:00
12:00
18:00
0:00
Nov. 3
6:00
12:00


Flaw leads
Case 4
Case 3

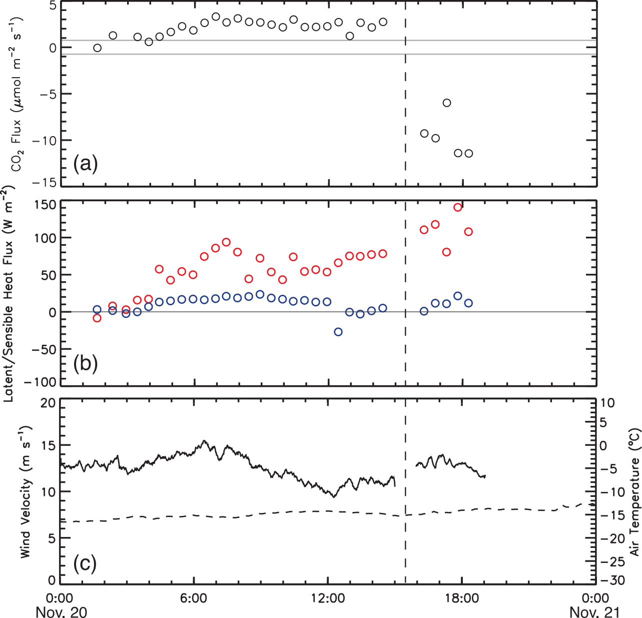

CO2 Flux (μmol m−2 s−1)
(a)
Latent/Sensible Heat Flux (W m−2)
(b)
Wind Velocity (m s−1)
Air Temperature (°C)
(c)
0:00
Nov. 20
6:00
12:00
18:00
0:00
Nov. 21

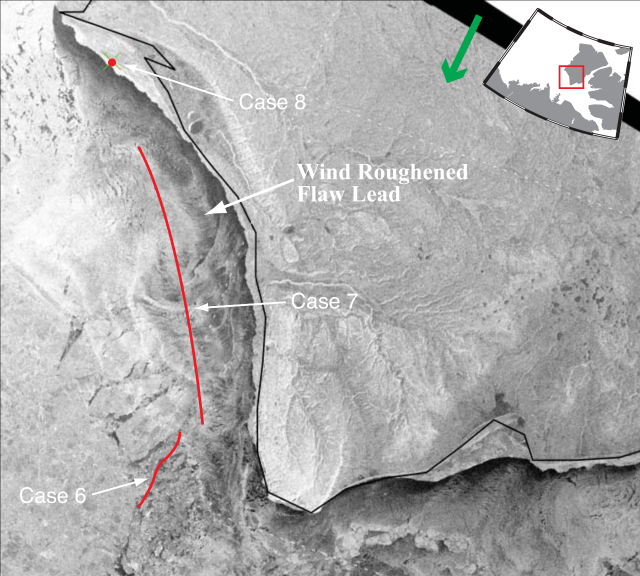
Case 8
Wind Roughened
Flaw Lead
Case 7
Case 6

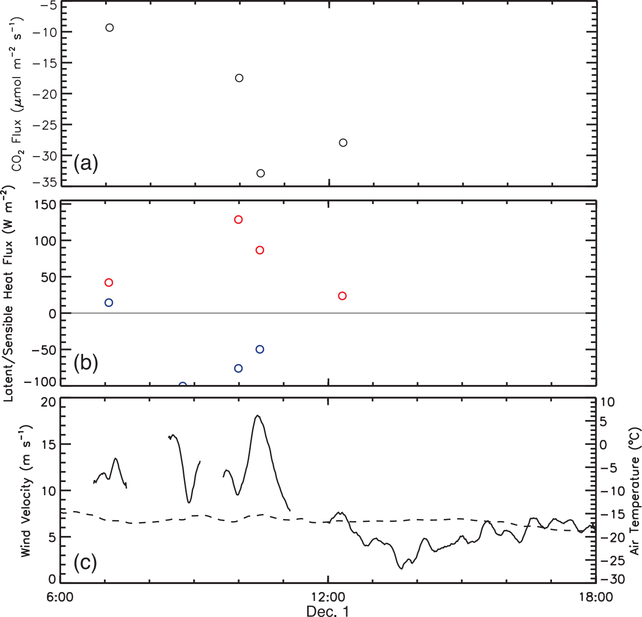

CO2 Flux (μmol m−2 s−1)
−5
−10
−15
−20
−25
−30
−35
(a)
Latent/Sensible Heat Flux (W m−2)
150
100
50
0
−50
−100
(b)
Wind Velocity (m s−1)
20
15
10
5
0
(c)
Air Temperature (°C)
10
5
0
−5
−10
−15
−20
−25
−30
6:00
12:00
18:00
Dec. 1

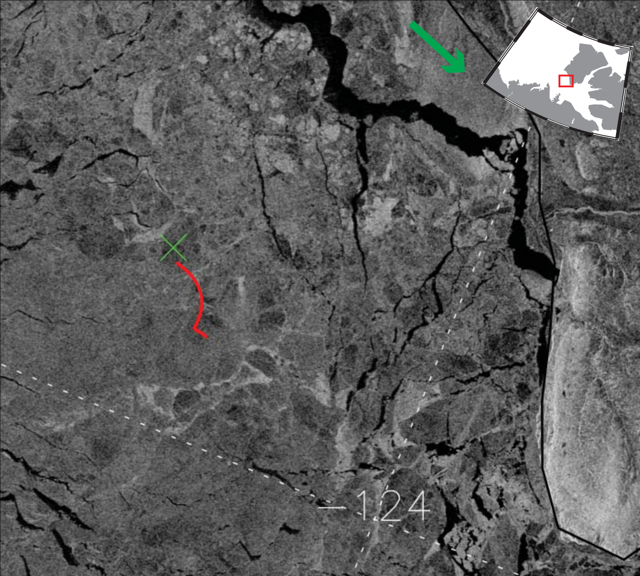
124

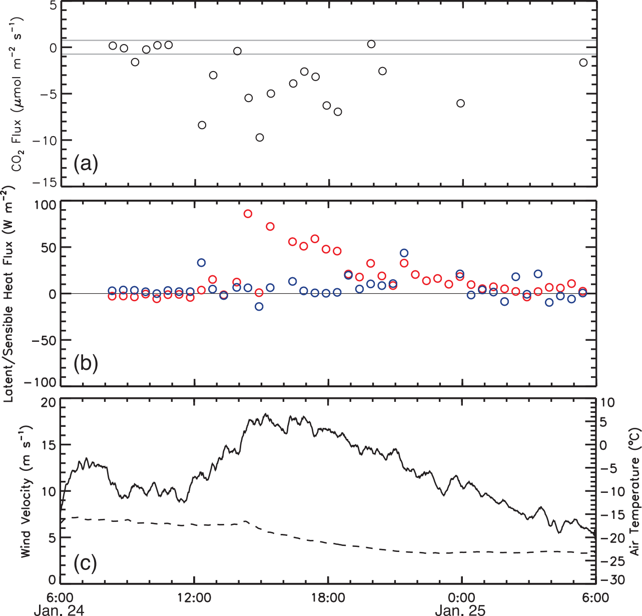

CO_2 Flux (μmol m^{-2} s^{-1})
5
0
−5
−10
−15
(a)
Latent/Sensible Heat Flux (W m^{-2})
100
50
0
−50
−100
(b)
Wind Velocity (m s^{-1})
20
15
10
5
0
Air Temperature (°C)
10
5
0
−5
−10
−15
−20
−25
−30
(c)
6:00
Jan. 24
12:00
18:00
0:00
Jan. 25
6:00

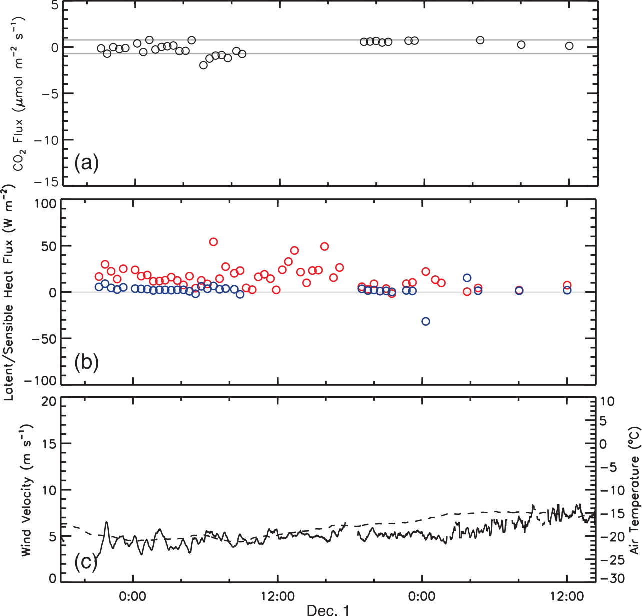
CO$_2$ Flux (μmol m^{-2} s^{-1})
(a)
Latent/Sensible Heat Flux (W m^{-2})
(b)
Wind Velocity (m s^{-1})
Air Temperature (°C)
(c)
0:00
12:00
0:00
12:00
Dec. 1

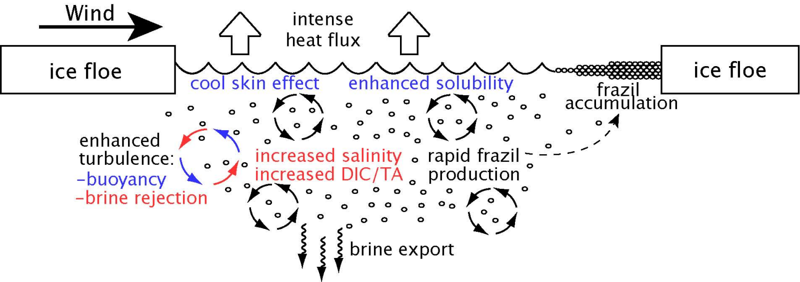
Wind
intense
heat flux
ice floe
ice floe
cool skin effect
enhanced solubility
frazil
accumulation
enhanced
turbulence:
-buoyancy
-brine rejection
increased salinity
increased DIC/TA
rapid frazil
production
brine export

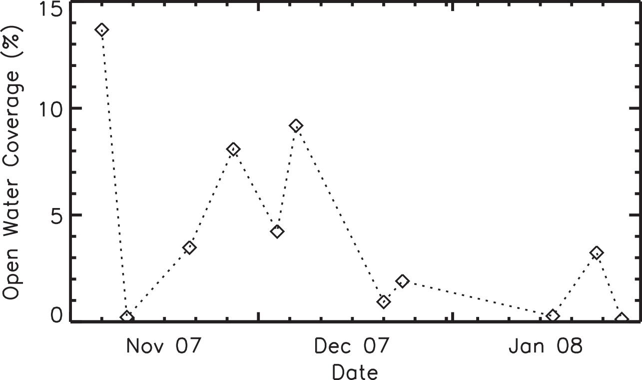
15
10
5
0
Open Water Coverage (%)
Nov 07
Dec 07
Jan 08
Date